Room-temperature heterodyne terahertz detection with quantum-level sensitivity

Ning Wang[1,3], Semih Cakmakyapan[1,3], Yen-Ju Lin[1], Hamid Javadi[2] and Mona Jarrahi [1*]

Our Universe is most radiant at terahertz frequencies (0.1–10.0 THz) (ref. [1]), providing critical information on the formation of the planets, stars and galaxies, as well as the atmospheric constituents of the planets, their moons, comets and asteroids[2–9]. The detection of faint fluxes of photons at terahertz frequencies is crucial for many planetary, cosmological and astrophysical studies[10–14]. For example, understanding the physics and molecular chemistry of the life cycle of stars and their relationship with the interstellar medium in galaxies requires heterodyne detectors with noise temperatures close to the quantum limit[15]. Near-quantum-limited heterodyne terahertz detection has so far been possible only through the use of cryogenically cooled superconducting mixers as frequency downconverters[15–18]. Here we introduce a heterodyne terahertz detection scheme that uses plasmonic photomixing for frequency downconversion to offer quantum-level sensitivities at room temperature. Frequency downconversion is achieved by mixing terahertz radiation and a heterodyning optical beam with a terahertz beat frequency in a plasmonics-enhanced semiconductor active region. We demonstrate terahertz detection sensitivities down to three times the quantum limit at room temperature. With a versatile design capable of broadband operation over a 0.1–5.0 THz bandwidth, this plasmonic photomixer has broad applicability to astronomy, cosmology, atmospheric studies, gas sensing and quantum optics.

Our heterodyne terahertz detection scheme is governed by new physical processes that enable quantum-level sensitivity, broad spectral bandwidth and high spectral resolution while operating at room temperature. Figure 1 shows the operation principles of our heterodyne terahertz detector. It consists of a plasmonic photomixer (that is, a photomixer with plasmonic contacts) integrated with a logarithmic spiral antenna on a photo-absorbing semiconductor substrate. The plasmonic photomixer is pumped by a heterodyning optical beam with beat frequency ω_{beat}. The geometry of the plasmonic contact electrodes, which are in the form of gratings, is chosen such that a y-polarized optical pump excites surface plasmon waves along the gratings to tightly confine the optical pump beam at the interface between the metallic gratings and semiconductor substrate. Therefore, the intensity of the optical pump beam, $I_{\text{pump}}(x,y,z)[1+\cos(\omega_{\text{beat}}t)]$, at the location (x,y,z), where t is time, and the photocarrier concentration inside the semiconductor substrate are substantially enhanced near the contact electrodes, as illustrated in Supplementary Fig. 1. When a terahertz radiation at angular frequency ω_{THz} is received by the logarithmic spiral antenna, a terahertz electric field is induced inside the semiconductor substrate, $E_{\text{THz}}(x,y,z)\cos(\omega_{\text{THz}}t)$, which drifts the photocarriers to the contact electrodes. The induced drift photocurrent is calculated as

$$I_{\text{drift}}(t)=$$

$$\frac{q\alpha\tau}{h\nu}\int_{V_{\text{total}}}I_{\text{pump}}(x,y,z)\left(\frac{\mu_{\text{n}}}{L_{\text{n}}(x,y,z)}+\frac{\mu_{\text{p}}}{L_{\text{p}}(x,y,z)}\right)E_{\text{THz}}(x,y,z)\,\mathrm{d}V$$

$$\times\frac{1}{2}\Re\left[\frac{2\mathrm{e}^{j\omega_{\text{THz}}t}}{1-j\omega_{\text{THz}}\tau}+\frac{\mathrm{e}^{j(\omega_{\text{beat}}+\omega_{\text{THz}})t}}{1-j(\omega_{\text{beat}}+\omega_{\text{THz}})\tau}+\frac{\mathrm{e}^{j|\omega_{\text{beat}}-\omega_{\text{THz}}|t}}{1-j\,|\omega_{\text{beat}}-\omega_{\text{THz}}|\,\tau}\right]\quad(1)$$

where q is the electron charge, α is the optical absorption coefficient in the semiconductor, τ is the carrier lifetime in the semiconductor, assumed to be the same for electrons and holes, $h\nu$ is the photon energy (h is Planck's constant and ν is the photon frequency), $\mu_{\text{n}}/\mu_{\text{p}}$ is the electron/hole mobility (where 'n' and 'p' stand for negative and positive charges, respectively), $L_{\text{n}}(x,y,z)/L_{\text{p}}(x,y,z)$ is the drift path distance of the electron/hole generated at the location (x,y,z) to the device contact electrodes, $\Re$ is the real part of the function, j is the imaginary unit, $\mathrm{d}V$ is the differential element of volume, and V_{total} is the total volume (derivation details are described in Supplementary Fig. 2).

The induced drift photocurrent has three frequency components at ω_{THz}, $\omega_{\text{beat}}+\omega_{\text{THz}}$ and $|\omega_{\text{beat}}-\omega_{\text{THz}}|$. By appropriately selecting the pump beat frequency relative to the received terahertz frequency, the frequency component at $|\omega_{\text{beat}}-\omega_{\text{THz}}|$ falls in the radio frequency (RF) range. Hereafter, we refer to this frequency component as the intermediate frequency (IF). As shown in equation (1), the induced IF photocurrent is directly proportional to the volume integral of

$$I_{\text{pump}}(x,y,z)\left(\frac{\mu_{\text{n}}}{L_{\text{n}}(x,y,z)}+\frac{\mu_{\text{p}}}{L_{\text{p}}(x,y,z)}\right)$$

Therefore, to achieve high terahertz-to-RF conversion efficiencies, it is desirable to generate the photocarriers at very short distances from the contact electrodes and boost the intensity of the optical pump beam, which generates the photocarriers near the contact electrodes. Excitation of surface plasmon waves along the contact electrode gratings at the optical pump wavelength facilitates achieving these goals. Since the excited surface plasmon waves are tightly confined at the interface between the metallic gratings and semiconductor substrate, the intensity of the optical pump beam coupled to the semiconductor substrate and the concentration of the photocarriers are both substantially enhanced in close proximity to the device contact electrodes, as illustrated in Supplementary Figs. 1 and 3.

[1]Electrical and Computer Engineering Department, University of California, Los Angeles, CA, USA. [2]Jet Propulsion Laboratory, California Institute of Technology, Pasadena, CA, USA. [3]These authors contributed equally: Ning Wang, Semih Cakmakyapan. *e-mail: mjarrahi@ucla.edu
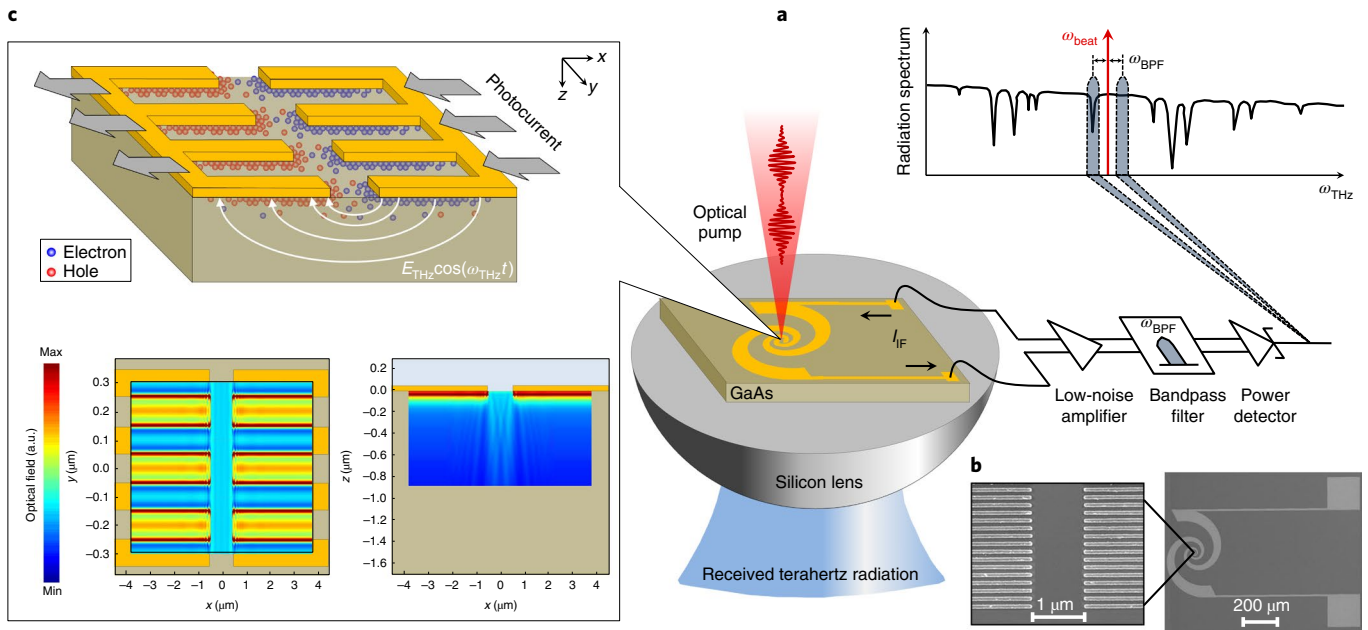
Fig. 1 | Principles of heterodyne terahertz detection through plasmonic photomixing. a, When the plasmonic photomixer is pumped by a heterodyning optical beam with a terahertz beat frequency, the received terahertz radiation near $\omega_{beat} + \omega_{BPF}$ is downconverted to an IF current, I_{IF}, at $|\omega_{beat} - \omega_{THz}|$, which can be easily detected by RF electronics. **b**, Scanning electron microscopy image of a fabricated plasmonic photomixer prototype. **c**, To achieve high terahertz-to-RF conversion efficiencies, two nanoscale titanium/gold gratings with a thickness of 50 nm, pitch of 200 nm, spacing of 100 nm and 300 nm-thick Si_3N_4 anti-reflection coating are used as the photomixer contacts to enhance the optical pump intensity at the contact/semiconductor interface through the excitation of surface plasmon waves. These plasmonic contact electrode gratings are designed to cover an $8 \times 8\,\mu m^2$ active area with a tip-to-tip gap of $1\,\mu m$. This design of plasmonic gratings provides a strong plasmonic enhancement when excited by a y-polarized optical pump beam at a wavelength of ~784 nm, as illustrated in the top view (x–y plane) and cross-sectional view (x–z plane) colour plots of the optical field in the gallium arsenide (GaAs) substrate, where the electric field intensity is shown in arbitrary units (a.u.) (see Methods and Supplementary Fig. 1).

Figure 1b shows a scanning electron microscopy image of a fabricated plasmonic photomixer prototype (see Methods for the fabrication process details). A short-carrier-lifetime semiconductor is used as the photo-absorbing substrate (that is, a low-temperature-grown gallium arsenide substrate with a 0.3 ps carrier lifetime) to recombine the slow photocarriers that degrade the terahertz-to-RF conversion efficiency. To achieve a broad spectral bandwidth, the geometry of the logarithmic spiral antenna is chosen to offer a radiation resistance of ~70 Ω and a negligible reactance over the 0.1–5.0 THz frequency range. Two nanoscale titanium/gold gratings are used as the plasmonic photomixer contacts, and their dimensions are chosen to enhance the optical pump intensity at the contact/semiconductor interface through the excitation of surface plasmon waves[19,20], as illustrated in Fig. 1c.

The induced IF signal by the plasmonic photomixer is routed through a low-noise amplifier and a bandpass filter, with an angular frequency bandwidth of ω_{BPF}, and is detected by an RF power detector, as illustrated in Fig. 1a. The frequency components at ω_{THz} and $\omega_{beat} + \omega_{THz}$ are substantially attenuated when propagating along the IF transmission lines. The detected RF power carries the received spectral information at $\omega_{beat} + \omega_{BPF}$ over a spectral bandwidth equal to the bandwidth of the bandpass filter. By tuning the optical pump beat frequency and recording the detected power, the received terahertz spectrum is extracted over a broad frequency range determined by the logarithmic spiral antenna bandwidth. Moreover, the received terahertz spectrum is resolved with a high spectral resolution determined by the bandwidth of the bandpass filter and the linewidth of the optical pump beam. The described heterodyne detector operates in a double sideband (DSB) mode of observation, where the spectral information of the desired terahertz frequency at $\omega_{beat} - \omega_{BPF}$ is measured together with that of the image frequency, $\omega_{beat} + \omega_{BPF}$.

Our heterodyne terahertz detection scheme offers transformative advantages over conventional techniques that use a Schottky diode, hot electron bolometer (HEB) or superconductor–insulator–superconductor (SIS) mixer together with a terahertz local oscillator for terahertz-to-RF downconversion[21–27]. The plasmonic photomixer is designed such that the IF output and noise powers have a quadratic and linear dependence on the optical pump power, respectively. As a result, the signal-to-noise ratio (SNR) and dynamic range can both be increased by boosting the optical pump power. By controlling the photomixer's SNR through the optical pump power level, we demonstrate terahertz detection with quantum-level sensitivities without the need for cryogenic cooling, which is required by SIS and HEB mixers to offer similar sensitivities. Another major advantage of our heterodyne terahertz detection scheme is that its spectral bandwidth is determined by the wavelength tuning range of the optical pump source. Therefore, it offers broad spectral bandwidths that cannot be achieved by conventional techniques because of the limited tunability of existing terahertz local oscillators. We demonstrate terahertz detection over the 0.1–5.0 THz frequency range with a spectral resolution and stability of less than 1 kHz through a single plasmonic photomixer. To achieve the same spectral bandwidth through conventional techniques, a large number of cryogenically cooled superconducting mixers and terahertz local oscillators operating over the 0.1–5.0 THz frequency range would be required to offer similar sensitivities.

The operation of the fabricated plasmonic photomixer as a heterodyne terahertz detector is first characterized at 0.55 THz (see Methods and Supplementary Fig. 4a). A ×2×3 frequency multiplier chain developed at the Jet Propulsion Laboratory (JPL) for the Herschel Space Observatory is used to provide the 0.55 THz radiation incident on the plasmonic photomixer. Two wavelength-tunable distributed-feedback (DFB) lasers are used to provide the heterodyning optical pump beam. Figure 2a shows the observed IF
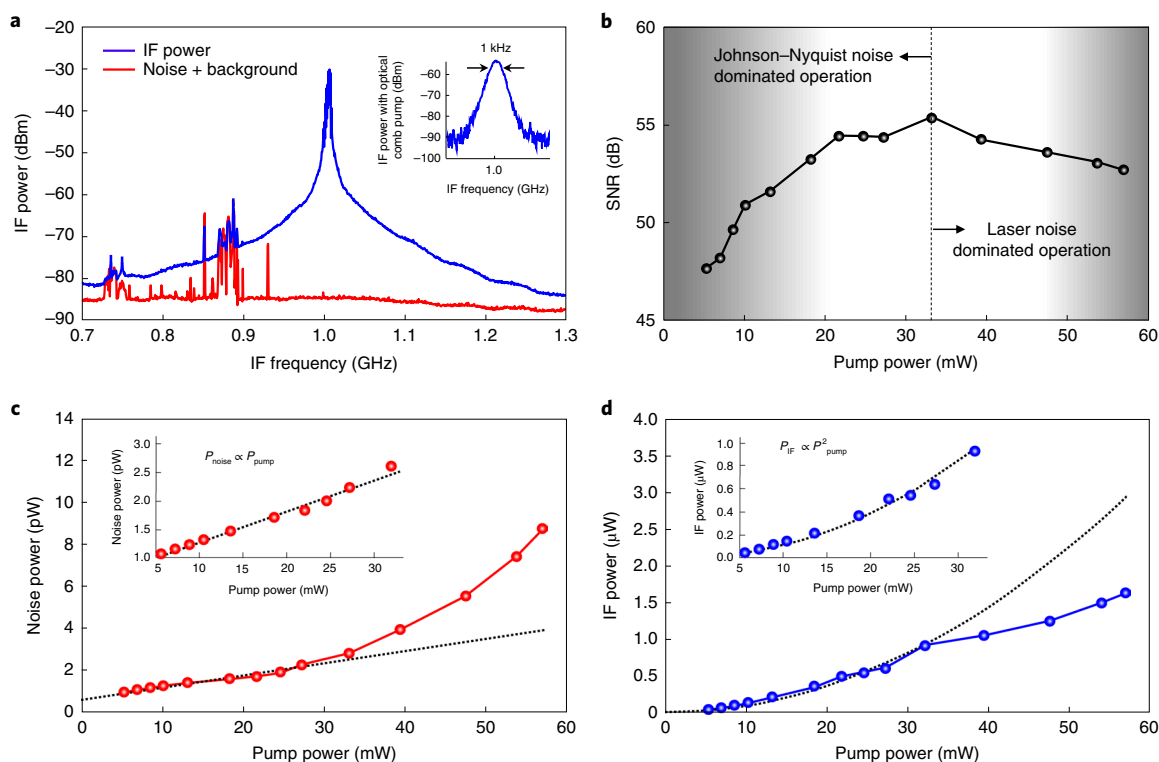
Fig. 2 | Terahertz-to-RF conversion using the fabricated plasmonic photomixer. a, The downconverted IF spectrum from 0.55 THz to 1 GHz (blue curve) and the IF noise/background in the absence of the 0.55 THz source (red curve) at an optical pump power of 33 mW from two DFB lasers. Inset: the IF spectrum when an optical comb from a titanium–sapphire mode-locked laser is used as the optical pump beam. **b–d**, The measured IF SNR (**b**), noise power, P_{noise}, (**c**) and IF power, P_{IF}, (**d**) as a function of the optical pump power, P_{pump}. The dashed lines show the theoretically predicted linear and quadratic dependence of the noise power and IF power on the optical pump power in **c** and **d**, respectively. A tunable attenuator is used to vary the optical pump power in these measurements. The IF noise and signal powers show a linear and quadratic dependence on the optical pump power below 33 mW, as illustrated in **c** and **d** insets with R^2 (coefficient of determination) fits of 98.5% and 99.1%, respectively.

spectrum centred at 1 GHz (blue curve) and the noise/background spectrum in the absence of the terahertz radiation (red curve). The lower spectral peaks observed near 750 MHz and 900 MHz are the background radio signals picked up by the IF transmission lines and cables. The observed IF signal has a linewidth of ~3 MHz, which is dominated by the linewidth of the two DFB lasers that provide the heterodyning optical pump beam[28] (see Methods). No observable change in the IF signal intensity is noticed when sweeping the IF centre frequency over the 1 GHz bandwidth of the IF amplifier by tuning the optical pump beat frequency over the 1 GHz bandwidth, implying an IF bandwidth of more than 1 GHz.

The linewidth of the IF signal, which also determines the spectral resolution of the heterodyne detection system, can be further reduced by using a heterodyning optical pump beam with narrower linewidth. To demonstrate the impact of the optical pump linewidth on the spectral resolution of the presented heterodyne detection system, a highly stable optical comb from a titanium–sapphire mode-locked laser is used as the optical pump beam (see Methods and Supplementary Fig. 4b). The observed spectrum near 1 GHz (Fig. 2a inset) has a linewidth of 1 kHz full-width at half-maximum, which is dominated by the linewidth of the 0.55 THz source. Therefore, the fabricated plasmonic photomixer enables heterodyne terahertz detection with resolutions of less than 1 kHz.

Another important specification of the optical pump beam that directly impacts the sensitivity and dynamic range of the plasmonic photomixer is the optical pump power. To demonstrate the impact of the optical pump power on the sensitivity and dynamic range of the plasmonic photomixer, the IF signal and noise powers of the plasmonic photomixer in response to the 0.55 THz source are

recorded at different optical pump powers, and the IF SNR is calculated by taking the ratio between the IF signal and noise powers at each optical pump power. The calculated IF SNR values shown in Fig. 2b indicate a linear increase in the SNR at optical powers below 33 mW and a reduction in the SNR at optical powers above 33 mW. This trend can be explained by different physical mechanisms affecting the photomixer noise and photocarrier dynamics inside the device's active area. At low optical pump powers, the device noise is dominated by Johnson–Nyquist noise[29]. Therefore, the IF noise power, which is inversely proportional to the photomixer resistance, increases linearly as a function of the optical pump power. The laser noise becomes more dominant at high optical pump powers, increasing the rate of the IF noise growth as a function of the optical pump power, as illustrated in Fig. 2c. Conversely, the IF signal power, which is quadratically proportional to the induced drift photocurrent, increases quadratically as a function of the optical pump power at low optical pump powers. The carrier screening effect becomes more dominant at high photocarrier concentrations, decreasing the rate of the IF signal growth as a function of the optical pump power, as illustrated in Fig. 2d.

The plasmonic photomixer sensitivity is characterized using the Y-factor method, which measures the IF response of the plasmonic photomixer to input noise sources from hot and cold loads (see Methods and Supplementary Fig. 4c). Unlike most studies that use a single hot/cold load for Y-factor measurements, multiple hot/cold loads are used in our sensitivity analysis to simultaneously assess the linearity of the detection system. Figure 3a,b shows the measured IF power in response to thermal loads varying between 77 K and 1,500 K with an optical pump power of 30 mW. The observed roll-off in the IF
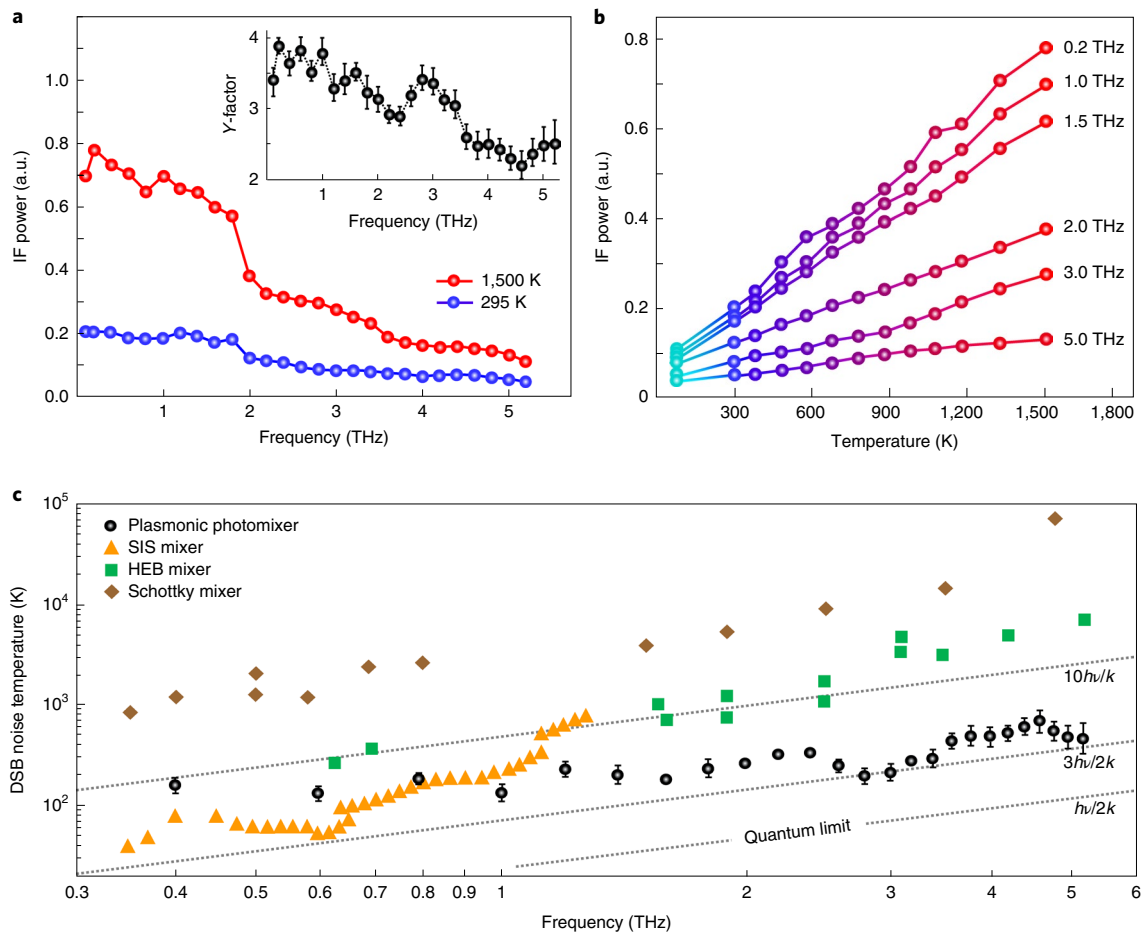
Fig. 3 | Noise temperature characteristics of the fabricated plasmonic photomixer. a, The measured IF power in response to 1,500 K/295 K hot/cold loads at an optical pump power of 30 mW over the 0.1–5.0 THz frequency range. Inset, the Y-factor values calculated as the measured IF power at 1,500 K divided by the measured IF power at 295 K. The error bars represent the maximum observed deviation in the calculated Y-factor values. The measurements are performed at frequencies away from strong water absorption lines. By sweeping the beat frequency of the heterodyning optical pump beam and recording the IF power, water absorption lines matching the HITRAN database[31] are observed. **b**, The measured IF power in response to thermal loads in the 77–1,500 K range at an optical pump power of 30 mW. **c**, DSB noise temperature values of the plasmonic photomixer compared with previously demonstrated Schottky diode mixers, HEB mixers and SIS mixers used in conventional heterodyne detectors[27]. The DSB noise temperature values are calculated as $(T_{eff(1,500)} - Y \times T_{eff(295)})/(Y-1)$, where $T_{eff(1,500)}$ and $T_{eff(295)}$ are the equivalent temperatures of a blackbody at 1,500 K and 295 K, respectively, according to the Callen–Welton definition. The error bars, which represent the maximum observed deviation in the calculated DSB noise temperature values, are attributed to the fluctuations in the optical pump power. The demonstrated noise temperature levels at lower frequencies are limited by the low radiation coupling to the used silicon lens with a 1.2 cm diameter.

power at higher frequencies is due to the plasmonic photomixer parasitics and antenna frequency response (Fig. 3a). As expected, a linear relation between the IF power and the load temperature is observed over the entire 77–1,500 K range (Fig. 3b). The Y-factor and DSB noise temperature values are calculated from the measured IF powers at 1,500 K/295 K hot/cold loads using the Callen–Welton effective hot/cold temperatures[30] (see Methods). Although 1,500 K and 295 K are used as the hot and cold loads, respectively, the linear dependence of the IF power on the load temperature (Fig. 3b) indicates that the same DSB noise temperature values can be achieved when using other hot/cold temperatures (Supplementary Fig. 5). DSB noise temperatures of 120–700 K are achieved in the 0.1–5.0 THz frequency range with an optical pump power of 30 mW at room temperature (Fig. 3c), corresponding to sensitivity values down to three times the quantum noise limit ($h\nu/2k$, where k is Boltzmann's constant).

Figure 3c compares the DSB noise temperature of the fabricated plasmonic photomixer with previously demonstrated Schottky diode, HEB and SIS mixers used in conventional heterodyne detectors[27] in the 0.3–5.0 THz frequency range. This comparison

indicates the superior performance of the presented plasmonic photomixer in offering noise temperatures lower than the cryogenically cooled HEB mixers and SIS mixers at frequencies above 0.8 THz (down to three times that of the quantum noise limit) without the need for a terahertz local oscillator and while operating at room temperature (see Methods). In particular, it is remarkable that the presented plasmonic photomixer offers lower DSB noise temperature values than the heterodyne detectors used in observatories such as Herschel (Heterodyne Instrument for the Far Infrared) and the Stratospheric Observatory for Infrared Astronomy (German Receiver for Astronomy at Terahertz Frequencies instrument), which use HEB mixers cooled at 4 K to achieve DSB noise temperature values of 1,000–1,500 K in the 1.6–1.9 THz frequency range and 2,000 K at 2.5 THz (refs. [15,16]). This performance is achieved by a single plasmonic photomixer and optical pump beam with a beat frequency tunability of 5.0 THz. To achieve similar sensitivities and spectral bandwidths through conventional techniques, a large number of cryogenically cooled SIS mixers, HEB mixers and terahertz local oscillators would be required[15–18].

The heterodyne terahertz detection scheme introduced here opens up new opportunities at the interface of quantum optics and terahertz photonics and offers a versatile experimental platform for different fundamental astronomical, cosmological and atmospheric studies (Supplementary Table 1). The presented plasmonic photomixer can be integrated with polarization-sensitive antennas (Supplementary Fig. 6) to determine minute anisotropies in the interstellar radiation polarization, which are crucial for understanding shock processes in the interstellar medium originating from supernova explosions and stellar winds. Ultimately, the plasmonic photomixer can be fabricated in an array, and a heterodyning optical beam can pump all the array elements simultaneously using a microlens array, integrated waveguide array or fibre bundle.

Methods

Photomixer fabrication. The plasmonic photomixer is fabricated on a low-temperature-grown GaAs substrate. The fabrication process starts with patterning two plasmonic contact electrode gratings, by electron beam lithography, followed by Ti/Au (5 nm/45 nm) deposition and liftoff. A 300 nm-thick Si_3N_4 anti-reflection coating layer is then deposited using plasma-enhanced chemical vapour deposition. Then, two contact vias (also known as a vertical interconnect access) are patterned by optical photolithography and etched through the Si_3N_4 layer by dry plasma etching. Finally, the logarithmic spiral antenna, IF transmission line and bonding pads are patterned using optical photolithography, followed by Ti/Au (50 nm/400 nm) deposition and liftoff. The fabricated plasmonic photomixer is mounted on a silicon lens (1.2 cm in diameter) glued onto a printed circuit board with an SMA (subminiature version A) connector. The device output pads are bonded to the leads of the SMA connector to extract the IF output signal. The printed circuit board is placed on a rotation mount to enable adjustment of the optical pump polarization. The silicon lens is glued to a tapered metallic cylinder (inner/outer diameter of 1.5 cm/4.5 cm and length of 2.5 cm) to assist radiation coupling at wavelengths comparable to or larger than the silicon lens dimensions.

Numerical simulations of the designed plasmonic gratings. A finite-element-method-based electromagnetic software package (COMSOL) is used to characterize the interaction of the optical pump with the designed nanoscale Ti/Au gratings with a thickness of 50 nm, pitch of 200 nm, spacing of 100 nm and 300 nm-thick Si_3N_4 anti-reflection coating. Supplementary Fig. 1a shows the power transmission of a y-polarized optical pump through the nanoscale gratings into the low-temperature-grown GaAs substrate, predicting an optical power transmission of 85% at an optical wavelength of ~784 nm. Since the optical transmission through the plasmonic gratings is accompanied by the excitation of surface plasmon waves, a large fraction of the photogenerated carriers is concentrated in close proximity to the contact electrode, as illustrated in Supplementary Fig. 1b.

Characterization of the heterodyne terahertz detector. The operation of the fabricated plasmonic photomixer as a heterodyne terahertz detector is characterized in response to radiation from a ×2×3 frequency multiplier chain developed at the JPL for the Herschel Space Observatory that upconverts the frequency of a Gunn oscillator (Millitech GDM-10 SN224) to 0.55 THz. To provide the heterodyning optical pump beam, the outputs of two wavelength-tunable DFB lasers with centre wavelengths of 785 nm and 780 nm (TOPTICA LD-0785–0080-DFB-1 and DLC-DL-PRO-780) are combined and amplified (TOPTICA BoosTA Pro) to provide a tunable optical beat frequency from 0.1 THz to 5.0 THz. The IF output of the plasmonic photomixer is amplified using a low-noise amplifier (Mini-Circuits ZRL-1150) and monitored by an electrical spectrum analyser. The schematic diagram of the experimental set-up is shown in Supplementary Fig. 4a.

To investigate the impact of the optical pump linewidth on the spectral resolution of the presented heterodyne detection system, a highly stable optical comb from a Ti:sapphire mode-locked laser with a comb spacing of 78 MHz is used as the optical pump beam. The schematic diagram of the experimental set-up is shown in Supplementary Fig. 4b.

The plasmonic photomixer sensitivity is characterized using the standard Y-factor method, which measures the IF response of the plasmonic photomixer to the input noise sources from hot and cold loads. Room-temperature and liquid-nitrogen-soaked TK Instruments Tessellating TeraHertz RAM absorber tiles are used to provide the thermal loads at 295 K and 77 K, respectively. Calibrated blackbody (Boston Electronics IR-563) and Globar sources (Thorlabs SLS203L) are used to provide the thermal loads in the 295–1,500 K range. The optical pump beam from the dual DFB laser system is modulated using an acousto-optic modulator (Gooch & Housego AOMO 3080-125) at a 100 kHz rate, and the output IF signal at ~1 GHz is detected by a power meter (Mini-Circuits ZX47-60LN) using a lock-in amplifier with the 100 kHz modulation reference frequency and a 1 s time constant/integration time. A low-noise amplifier (Mini-Circuits ZRL-1150) and a bandpass filter (Mini-Circuits ZVBP-909) with a 15 MHz bandwidth are used to further condition the IF signal before the power meter. The measurements

are performed in air, without the use of any vacuum or purging. The schematic diagram of the experimental set-up is shown in Supplementary Fig. 4c.

Noise temperature calculation. The output noise of a heterodyne detector is determined by both the input noise to the detector, N_i, and the noise produced by the detector, N_s, given by $N_s = kT_sB$, where B is the detector bandwidth and T_s is the noise temperature of the detector. It should be emphasized that T_s is not the physical temperature of the detector, but rather is an equivalent temperature that produces the same amount of noise. As a result, T_s can be lower than the environmental temperature for a well-designed high-sensitivity detector. One common way to measure the detector's noise temperature is the Y-factor method, which measures the ratio of the detector output to the input noise sources from a hot and cold load

$$Y = \frac{N_s + N_{i(hot)}}{N_s + N_{i(cold)}} \tag{2}$$

where $N_{i(hot)}$ and $N_{i(cold)}$ are the input noise powers from the hot and cold loads, respectively. The equivalent input noise power from the detector is calculated from the measured Y-factor

$$N_s = \frac{N_{i(hot)} - YN_{i(cold)}}{Y - 1} \tag{3}$$

where the noise powers from the hot/cold loads are given according to the Callen and Welton law

$$N_i = kTB\left[\frac{\frac{h\nu}{kT}}{\exp\left[\frac{h\nu}{kT}\right] - 1}\right] + \frac{h\nu}{2}B \tag{4}$$

where $h\nu/2$ is the quantum noise present even at absolute zero temperature and T is the physical temperature of the thermal load. Therefore, the equivalent input noise temperature of the detector is calculated as

$$T_s = \frac{T_{eff(hot)} - YT_{eff(cold)}}{Y - 1} \tag{5}$$

where $T_{eff(hot)}$ and $T_{eff(cold)}$ are the equivalent noise temperatures of the hot and cold loads, respectively. The equivalent noise temperature of a load at temperature T is calculated as

$$T_{eff} = T\left[\frac{\frac{h\nu}{kT}}{\exp\left[\frac{h\nu}{kT}\right] - 1}\right] + \frac{h\nu}{2k} \tag{6}$$

Minimum number of detectable photons. The output noise of a heterodyne detector when operating at a physical temperature T_0 is given by

$$N_0 = (N_i + N_s)G = kT_sBG + kT_0BG\left[\frac{\frac{h\nu}{kT_0}}{\exp\left[\frac{h\nu}{kT_0}\right] - 1}\right] + \frac{h\nu}{2}BG \tag{7}$$

where G is the gain of the detector. Conversely, the detector output power for a received input signal power of S_i is given by

$$S_0 = GS_i \tag{8}$$

Therefore, the SNR at the detector output is

$$SNR = \frac{S_0}{N_0} = \frac{S_i}{kT_sB + kT_0B\left[\frac{\frac{h\nu}{kT_0}}{\exp\left[\frac{h\nu}{kT_0}\right] - 1}\right] + \frac{h\nu}{2}B} \tag{9}$$

Assuming that an SNR of 1 is required for the minimum detectable signal, the minimum number of detectable photons is calculated as

$$\frac{kT_s}{h\nu} + \frac{kT_0}{h\nu}\left[\frac{\frac{h\nu}{kT_0}}{\exp\left[\frac{h\nu}{kT_0}\right] - 1}\right] + \frac{1}{2} \tag{10}$$

Therefore, the minimum number of detectable photons is determined by both the detector's physical temperature and the detector's noise temperature (which can be lower than the detector's physical temperature). At low terahertz frequencies

($h\nu \ll kT_0$) the minimum number of detectable photons is dominated by the input thermal noise to the detector. However, at higher terahertz frequencies at which the photon energy becomes comparable or larger than the input thermal noise to the detector, the minimum number of detectable photons is dominated by the detector's noise temperature. Therefore, single-photon detection sensitivities can be achieved at higher terahertz frequencies. For our fabricated plasmonic photomixer prototype, which offers a DSB noise temperature of ~1.5 $h\nu/k$ at 3 THz, the minimum number of detectable terahertz photons at room temperature (295 K) and 77 K are four and three, respectively. Here, we assume the same device noise temperature at 295 K and 77 K. However, since the device noise is dominated by the Johnson–Nyquist noise, lower device noise temperatures and minimum numbers of detectable terahertz photons are expected at 77 K.

Linewidth of the heterodyning optical pump. The spectrum of the heterodyned optical pump beam can be calculated from the spectra of the two DFB lasers forming the optical pump beam. The spectral profiles of the two DFB lasers used in our set-up, $f_{DFB1}(\omega)$ and $f_{DFB2}(\omega)$, are modelled by Gaussian functions with centre frequencies of ω_{DFB1} and ω_{DFB2} and $1/e^2$ linewidths of $4\sigma_{DFB1}$ and $4\sigma_{DFB2}$, respectively.

$$f_{DFB1}(\omega) = \frac{1}{\sqrt{2\pi}\,\sigma_{DFB1}} \exp\left(-\frac{(\omega-\omega_{DFB1})^2}{2\sigma_{DFB1}^2}\right) \tag{11}$$

$$f_{DFB2}(\omega) = \frac{1}{\sqrt{2\pi}\,\sigma_{DFB2}} \exp\left(-\frac{(\omega-\omega_{DFB2})^2}{2\sigma_{DFB2}^2}\right) \tag{12}$$

Therefore, the electric field of the heterodyned optical pump beam, which is the superposition of the electric fields of the two DFB laser beams, E_{DFB1} and E_{DFB2}, is calculated as

$$E_{pump}(t) = E_{DFB1} + E_{DFB2} = E_0 \int \sqrt{f_{DFB1}(\omega)}\, e^{j\omega t} d\omega + E_0 \int \sqrt{f_{DFB2}(\omega)}\, e^{j\omega t} d\omega \tag{13}$$

where E_0 is the electric field of the balanced DFB lasers. As a result, the power spectrum of the heterodyned optical pump beam at the beat frequency of the two DFB lasers is calculated as

$$P_{pump}(\omega) = \frac{|E_0|^2}{2\eta_0} \frac{1}{\sqrt{2\pi}\,\sigma_{pump}} \exp\left(-\frac{(\omega-\omega_{THz})^2}{2\sigma_{pump}^2}\right) \tag{14}$$

where η_0 is the characteristic impedance of free space and ω_{THz} is the angular beat frequency ($\omega_{DFB1} - \omega_{DFB2}$) set to be in the terahertz range. Therefore, the resulting heterodyned optical pump beam has a Gaussian spectrum with a $1/e^2$ linewidth of $4\sigma_{pump}$, where $\sigma_{pump} = (2\sigma_{DFB1}^2 + 2\sigma_{DFB2}^2)^{1/2}$.

Data availability
The authors declare that all data supporting the conclusions of the manuscript are present in the manuscript and the supplementary materials.

References
1. Neugebauer, G. et al. Early results from the Infrared Astronomical Satellite. *Science* **224**, 14–21 (1984).
2. Mahieu, E. et al. Recent Northern Hemisphere stratospheric HCl increase due to atmospheric circulation changes. *Nature* **515**, 104–107 (2014).
3. Manney, G. L. et al. Unprecedented Arctic ozone loss in 2011. *Nature* **478**, 469–475 (2011).
4. Solomon, S. et al. Contributions of stratospheric water vapor to decadal changes in the rate of global warming. *Science* **327**, 1219–1223 (2010).
5. Phillips, T. G. & Keene, J. Submillimeter astronomy (heterodyne spectroscopy). *Proc. IEEE* **80**, 1662–1678 (1992).
6. Hartquist, T. W. & Williams, D. A. *The Molecular Astrophysics of Stars and Galaxies* (Oxford Univ. Press, 1998).
7. van Dishoeck, E. F. & Blake, G. A. Chemical evolution of star-forming regions. *Annual Rev. Astron. Astrophys.* **36**, 317–368 (1998).
8. Dutrey, A., Guilloteau, S. & Guelin, M. Chemistry of protosolar-like nebulae: the molecular content of the DM Tau and GG Tau disks. *Astron. Astrophys.* **317**, L55–L58 (1997).
9. Biver, N. et al. Evolution of the outgassing of Comet Hale-Bopp (C/1995 O1) from radio observations. *Science* **275**, 1915–1918 (1997).
10. Hartogh, P. et al. Ocean-like water in the Jupiter-family comet 103P/Hartley 2. *Nature* **478**, 218–220 (2011).
11. Küppers, M. et al. Localized sources of water vapour on the dwarf planet (1) Ceres. *Nature* **505**, 525–527 (2014).
12. Brünken, S. et al. H_2D^+ observations give an age of at least one million years for a cloud core forming Sun-like stars. *Nature* **516**, 219–221 (2014).
13. Falgarone, E. et al. Large turbulent reservoirs of cold molecular gas around high-redshift starburst galaxies. *Nature* **548**, 430–433 (2017).
14. Hogerheijde, M. R. et al. Detection of the water reservoir in a forming planetary system. *Science* **334**, 338–340 (2011).
15. De Graauw, T. et al. The Herschel–Heterodyne Instrument for the Far-Infrared (HIFI). *Astron. Astrophys.* **518**, L6 (2010).
16. Putz, P. et al. Terahertz hot electron bolometer waveguide mixers for GREAT. *Astron. Astrophys.* **542**, L2 (2012).
17. Heyminck, S. et al. GREAT: the SOFIA high-frequency heterodyne instrument. *Astron. Astrophys.* **542**, L1 (2012).
18. Wootten, A. & Thompson, A. R. The Atacama Large Millimeter/submillimeter Array. *Proc. IEEE* **97**, 1463–1471 (2009).
19. Berry, C. W., Wang, N., Hashemi, M. R., Unlu, M. & Jarrahi, M. Significant performance enhancement in photoconductive terahertz optoelectronics by incorporating plasmonic contact electrodes. *Nat. Commun.* **4**, 1622 (2013).
20. Yardimci, N. T. & Jarrahi, M. Nanostructure-enhanced photoconductive terahertz emission and detection. *Small* **14**, 1802437 (2018).
21. Wengler, M. J. Submillimeter-wave detection with superconducting tunnel diodes. *Proc. IEEE* **80**, 1810–1826 (1992).
22. Gao, J. R. et al. Terahertz superconducting hot electron bolometer heterodyne receivers. *IEEE Trans. Appl. Supercond.* **17**, 252–258 (2007).
23. Kloosterman, J. L. et al. Hot electron bolometer heterodyne receiver with a 4.7 THz quantum cascade laser as a local oscillator. *Appl. Phys. Lett.* **102**, 011123 (2013).
24. Crowe, T. W. et al. GaAs Schottky diodes for THz mixing applications. *Proc. IEEE* **80**, 1827–1841 (1992).
25. Zmuidzinas, J. & Richards, P. L. Superconducting detectors and mixers for millimeter and submillimeter astrophysics. *Proc. IEEE* **92**, 1597–1616 (2004).
26. Semenov, A. D. et al. Superconducting hot-electron bolometer mixer for terahertz heterodyne receivers. *Trans. Appl. Supercond.* **13**, 168–171 (2003).
27. Hubers, H. W. Terahertz heterodyne receivers. *IEEE J. Sel. Top. Quantum Electron.* **14**, 378–391 (2008).
28. Yang, S.-H. & Jarrahi, M. Spectral characteristics of terahertz radiation from plasmonic photomixers. *Opt. Exp.* **23**, 28522–28530 (2015).
29. Wang, N. & Jarrahi, M. Noise analysis of photoconductive terahertz detectors. *J. Inf. Mill. THz Waves* **34**, 519–528 (2013).
30. Kerr, A. R. Suggestions for revised definitions of noise quantities, including quantum effects. *Trans. Microw. Theory Tech.* **47**, 325–329 (1999).
31. Gordon, I. E. et al. The HITRAN2016 molecular spectroscopic database. *J. Quant. Spect. Rad. Transf.* **203**, 3–69 (2017).

Author contributions
N.W. designed and fabricated the device prototypes and performed the heterodyne detector characterization measurements at the University of California, Los Angeles. S.C. performed the noise temperature measurements at the University of California, Los Angeles. Y.-J.L. designed and fabricated the IF circuits. H.J. assisted with project supervision and performed the spectral resolution characterization measurements at JPL. M.J. supervised the project and wrote the manuscript. All authors discussed the results and commented on the manuscript.

Competing interests
The authors declare no competing interests.

Additional information
Supplementary information is available for this paper at https://doi.org/10.1038/s41550-019-0828-6.

Reprints and permissions information is available at www.nature.com/reprints.

Correspondence and requests for materials should be addressed to M.J.

Peer review information: *Nature Astronomy* thanks Heinz-William Huebers, Juerg Leuthold and the other, anonymous, reviewer(s) for their contribution to the peer review of this work.

Publisher's note: Springer Nature remains neutral with regard to jurisdictional claims in published maps and institutional affiliations.